Proceedings of the ASME 2023 42nd International Conference on Ocean, Offshore and Arctic Engineering
OMAE2023
June 11-16, 2023, Melbourne, Australia

OMAE2023-102185

DYNAMIC ANALYSIS OF LAUNCHING AND RECOVERING ROV

Yulin Deng[1] **Xiudi Ren[2]** **Martin Nuernberg[4]** **Longbin Tao[1,3]**

1. Department of Naval Architecture, Ocean and Marine Engineering, University of Strathclyde, Glasgow, United Kingdom
2. PowerChina Huadong Engineering Corporation Limited. Hangzhou, Zhejiang, China
3. School of Naval Architecture and Ocean Engineering, Jiangsu University of Science and Technology, Zhenjiang, China
4. Technology for Advanced Offshore Solutions, Edinburgh, United Kingdom

ABSTRACT

During operation and maintenance of the offshore wind farms, some regular inspections for the wind turbines are performed by remotely operated underwater vehicles (ROV) and service operation vessels (SOV). However, the ROV often experiences excessive motions as it passes through wave zone due to wave-ROV interaction combined with free surface effects. These movements can cause rope slack and sudden loading, which may damage umbilical components and endanger ROV operation.

This study focuses on experimental measurements and numerical prediction of the dynamic tension in the umbilical during launch and recovery of ROV passing through wave zone under different environmental conditions combined with winching process and ship motions. A coupled offshore vessel, umbilical and ROV hydrodynamic analysis for launching and recovering ROV, which is a typical offshore wind farm service operation, is carried out with coupling characteristics being examined.

The numerical results are validated by the 1:10 scale model test measurements on the ROV. The numerical simulation shows ROV experiences larger umbilical tension in recovery process than that in launch process in general. It is found that the tension in the cable is primarily determined by the strength and direction of wind and wave, and the change of winch speed does not significantly impact on the maximum tension in umbilical within the operational range examined.

Keywords: Remotely operated underwater vehicle (ROV); Launch and recovery; Offshore wind turbine; Maintenance

1. INTRODUCTION

Wind energy, as a zero-emission energy source of pollutants and greenhouse gases, is becoming more and more popular around the world. The North Sea is an important source of wind energy in Europe. According to offshore wind farm map and database of 4C Offshore, there are more than 41 wind farms in the North Sea, with about 2630 turbines and a total capacity of about 100,133 MW [1].

As the number of installed offshore wind turbines increases, there is a high demand for service support vessels to perform the necessary and regular maintenance and inspection tasks required for the safe operation of offshore wind farms. Most operators use vessel-based inspection systems for periodic inspections and maintenance related to scour, corrosion, weld, and structures. The assistance of a remotely operated vehicle (ROV) is required in most offshore operations such as platform inspection, pipeline inspection and subsea facilities [2].

The support vessel and offshore structure are connected by utilizing a single mooring to achieve a relatively stable state around the foundation under the wind, wave, swell and current forces. This allows the ROV to be deployed over the stern of the vessel, conducting sub-sea operations from around 30 - 45 meters [3].

The working procedure of ROV can be divided into five main stages in sequence: launch, descend, operation, ascend, and recovery. During the launch and recovery phases, the ROV achieves ascent and descent in the wave zone by gradually extending and reducing the length of the cable [4]. There is an interaction between the ROV and the ocean waves, which is also exacerbated by the motion of the ship caused by the waves. This combination of wave, vessel and ROV motion can cause slack in

the cable, often followed by a rapid taut. It will greatly increase the tension in the cable, which may exceed safe working loads, leading to premature failure of the cable and injury to the operators [5].

DNV recommended practice provides a simplified method to analyze the hydrodynamic forces of offshore connection system during lifting through wave zone. In the simplified method, the slack sling criterion is determined by the dynamic amplification factor of the cable force, that is the ratio of the total force to the static force, during the recovery phase of the system [6]. However, some literatures [7-8] show that the DNV recommended practice often leads to overestimated results by comparing the results of simplified method and numerical simulation.

In numerical simulation, launch and recovery of ROV can be simulated by establishing appropriate numerical models of the vessel, connection system, and ROV system, so that connection tension and hydrodynamic analysis can be performed through time-domain analysis. ROV launch and recovery can be simulated by utilizing appropriate numerical models of the vessel, cable and ROV, allowing for more appropriate structural and hydrodynamic analysis. Valen conducted research and showed that the operating limit of the studied ROV is reasonable by comparing the time domain results from SIMO software with the results from DNV specification [9]. By comparing the numerical simulation results of ROV lift operation in OrcaFlex and SIMO, Bjerkholt showed that simulating ROV launch and recovery in a time domain simulation program is another good solution compared to the simplified approach in DNV recommendations [10].

Jia and Agrawal introduced a novel fluid-structure interaction model for the descent phase of large submarine structures and used commercial CFD software to analyze the wave-structure interaction in the wave zone during installation [11]. During the lifting process, the generated snap load in cable is the main concern, so it is necessary to estimate the probability of sudden loading events and the magnitude of the tension reasonably and accurately. Thursen et al. studied the probability of lifting wire relaxation and nonlinear dynamic tension due to transient loads during offshore lifting operations [12]. Lubis conducted experiments using a 1:10 scale model of a working-scale ROV in a wave flume. The study measured the added mass and drag coefficient of the ROV passing through the wave zone, focusing on the effects of vessel motion and winch speed [13].

While typical offshore support vessels operating in conventional oil and gas industry are rather large, as one of the attempts to reduce the cost, the offshore renewable industry tends to use relatively small and more accessible vessels for the operation and maintenance of offshore wind farms. For secure and safe operation, the main objective of this study is to investigate the effect of various combinations of crane speed, different environmental conditions and ship motion on the instantaneous load magnitude, and the results obtained by modelling launch and recovery of ROV in the time domain simulation software Sesam. The developed numerical model was validated with 1:10 scale model scale experiment results in a wave flume, thereby determining the safe operating window for a working-class ROV to pass through the wave zone.

2. METHODOLOGY

The simulation work is carried out using a computer program called Simulation of Marine Operations (SIMO), which can perform motion, position and force behaviours between floating systems and suspended loads. In SIMO, the equations of motion of one or more object systems can be simplified as follows:

$$M\ddot{x} + C\ddot{x} + D_1\dot{x} + D_2 f(\dot{x}) + K_s x = q_{ex}(t, x, \dot{x}) \quad (1)$$

where M and C give the frequency dependent mass matrix and frequency dependent potential damping matrix, D_1 and D_2 represent linear and quadratic damping matrix, K_s is position dependent hydrostatic stiffness matrix, and q_{ex} is exciting forces.

In SIMO, complex subsea structures can be modelled by different elongated elements. The forces acting on the body are obtained by calculating, superimposing, and transferring the forces on each slender element. Each slender element is composed of several different strips, each of which requires the calculation of structural mass, additional mass, and external loads from buoyancy, environment, and slamming forces. The equations of motion and force balance for each strip are shown in the below:

$$F = (m + m_h)\ddot{x} + (\rho V + m_h)\ddot{\zeta} + v_r \frac{dm_h}{dt} + B_L v_r + B_Q v_r |v_r| + \rho g V \quad (2)$$

Inertial force is a function of structural mass, added mass and acceleration, where the relationship between the inertia coefficient C_m and the added mass coefficient C_a is

$$C_m = 1 + C_a \quad (3)$$

The drag term in SIMO is defined as a combination of linear and quadratic drag [14]. At low Keulegan-Carpenter number KC, linear damping B_1 and quadratic damping B_2 are represented as functions of the non-dimensional linear and quadrat damping coefficients b_1 and b_2, as shown in below:

$$B_1 = \frac{2\rho A_p \sqrt{2gD}}{3\pi^2} b_1 \quad (4)$$

$$B_2 = \frac{1}{2}\rho A_p b_2 \quad (5)$$

where A_p is horizontal projected area of object.

In this paper the JONSWAP spectrum is used to describe stochastic waves in the North Sea. According to the recommended of DNV, a reasonable JONSWAP spectrum has the following relationship between the significant wave height H_s and the spectrum peak period T_p:

$$3.6 \leq \frac{T_p}{\sqrt{H_s}} \leq 5 \quad (6)$$

The specific parameter selection will be discussed in the section 3.2.

3. MODEL SETUP OF THE OFFSHORE SUPPORT VESSEL AND ROV SYSTEM

3.1 Offshore support vessel

The vessel employed in the study is an offshore support vessel called the Fortuna Kingfisher, which has been specially retrofitted to perform inspection, maintenance and repair work on facilities located below the surface. The main dimensions of the Fortuna Kingfisher are shown in Table 1.

TABLE 1: Main dimensions of Fortuna Kingfisher

Main Dimensions	Unit	Value
Length Overall	m	38.92
Length between Perpendiculars	m	32.10
Length Waterline	m	34.60
Breadth Moulded	m	9.20
Depth Moulded	m	4.50
Draught Design Water Line	m	3.10
Displacement at Design Water Line	m^3	495.0
Lightship Mass	t	393.0
LCG from AP	m	15.47
VCG from BL	m	4.25

The established panel model of offshore support vessel is shown in Figure 1.

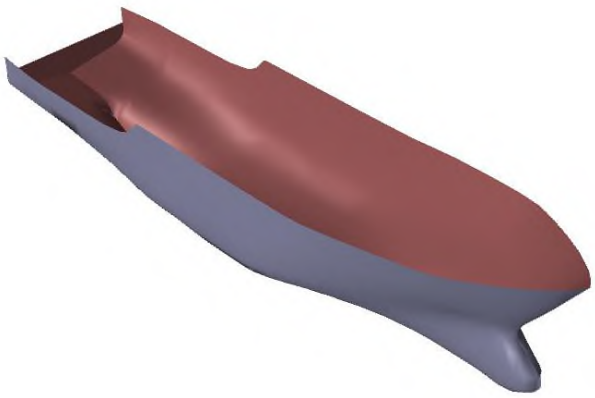

FIGURE 1: Visualization of the panel model of offshore support vessel

3.2 ROV and TMS system

Fortuna Kingfisher is equipped with a work class ROV named Seaeye Cougar-XT. Table 2 and 3 show the main dimensions of the ROV and the tether management system (TMS), and the mass skid manipulators is contained in the ROV structure mass. The current operational limit for ROV and TMS system is a significant wave height of 1.0 m.

TABLE 2: Main dimensions of Seaeye Cougar-XT

Main Dimensions	Unit	Value
Length	m	1.515
Width	m	1.000
Height	m	0.79
Mass	kg	409
Displacement	m^3	0.481
Porosity		0.600

TABLE 3: Main dimensions of TMS

Main Dimensions	Unit	Value
Length	m	1.79
Width	m	1.49
Height	m	2.30
Mass	kg	1416.8
Displacement	m^3	0.413
Porosity		0.933

The SIMO theory manual recommends the subsea structures can be modelled by simple structures consisting of slender elements in SIMO. The TMS consists of 45 slender elements, while the ROV consists of 26 different slender elements. Each slender element affects the scale, total mass and buoyancy of the system structure, so the properties of the slender elements adjusted and tuned to match the main dimensions of the ROV and TMS system. The slender element model of ROV and TMS system is shown in Figure 2.

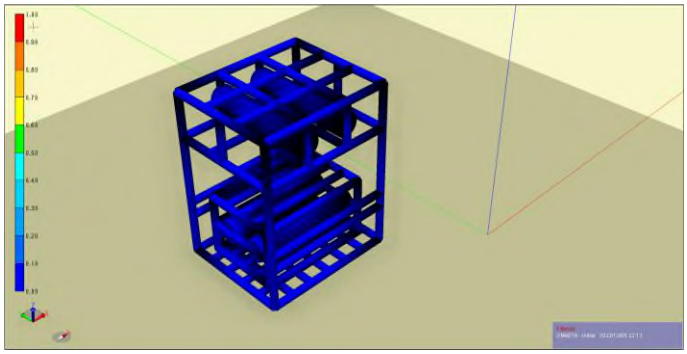

FIGURE 2: Visualization of the slender element model of ROV and TMS system

To reveal the motion and force response of the system, some hydrodynamic coefficients need to be input to estimate the hydrodynamic force acting on the loaded object, thus simulating the fluid dynamics and structural properties as accurately as possible. The literatures [8-10] show that semi-empirical methods can be used to determine the forces under various conditions, and the common practice is to use the additional mass of the non-perforated structure to estimate the additional mass of the perforated structure, and then multiply it by the reduction factor to consider the impact of the perforation.

Sayer conducted model tests of Super Scorpio ROV and concluded that the inertia coefficient of a working class ROV is in the range of 1.4-1.6, while the same experiments on a solid

box showed the inertia coefficient is in the range of 1.5 - 1.9 [15]. Kopsov and Sandvik also concluded that perforation reduces the added mass of the object and increases the drag contribution [16,17]. Since the main dimensions of Seaeye Cougar is slightly smaller than the Super Scorpio, and the solid box of Seaeye Cougar has fewer perforations, it is assumed that the inertia coefficient of the ROV and TMS system is in the range of 1.5-1.8. Another study by Sayer showed that the inertia coefficient of the Super Scorpio increases averaged 10% due to approaching the free surface of water [18]. Then the inertia coefficient is adjusted to be in the 1.65-1.98 range, which means that the added mass coefficient is in the 0.65-0.98 range according to equation 3, with a final conservative estimate of 0.8.

Øritsland and Lehn provided extensive hydrodynamic data for typical subsea modular structures [19]. The fullness factor V/LBH of the ROV system is 0.40, which is similar to the structure 10 fullness factor 0.32, indicating that the characteristics of the two are similar. The parameters of structure 10 in the sway and heave directions were obtained based on the literature summary and are shown in Table 4.

TABLE 4: Parameters of structure 10

Motion	C_a	b_1	b_2	C_{ds}
Sway	0.75	0.24	1.89	0.93
Heave	0.75	0.24	1.89	0.93

The C_{ds} is steady state drag coefficient. The structure 10 has a smaller the added mass coefficient than the ROV system. According to Sayer, the drag coefficient of the object makes an increase of 25% when it is close to the water surface [20]. Therefore, it is necessary to adjust the dimensionless non-dimensional linear and quadratic damping coefficients with appropriate increases, and the final values are 0.30 and 1.90, respectively. Based on formulas 4 and 5, the values of B_1 and B_2 can be obtained.

3.3 Lifting system

The ROV and TMS system is connected to the service vessel by an umbilical cable and the lifting system performs the raising and lowering operations by means of a crane. The connecting cable is a 3-strand Superflex polyester rope with a size of 24 mm and the main parameters are shown in Table 5. The properties of crane and cable were obtained from Randers Reb and O.S. Energy Ltd.

TABLE 5: Main dimensions of lifting system

Main Dimensions	Unit	Value
Outer diameter	mm	24
Mass/unit length	kg/m	0.260
Wire cross section stiffness	N	$3.9 \cdot 10^7$
Max winch speed	m/s	0.8

The lifting system is modelled as a simple wire coupling consisting of linear springs, and it can be conveniently used in lifting operations with a single point of attachment on the object being lifted. According to the SIMO manual, material damping is usually about 1-2% of the axial stiffness, and the flexibility of the lifting system is the reciprocal of the axial stiffness.

3.4 Environment condition

Offshore crane operations are assumed to be performed within 30 minutes. According to the operating limit of ROV, the equation 6 and the weather forecast of the wind farm in the field, the specific environmental conditions for ROV launch and recovery are selected as shown in Table 6.

TABLE 6: Conditions of the respective sea state

Condition	Direction	Value
Unit	degree	m/s
Wind	125	5.8
Wave	180	1.0
Swell	250	0.2
Current	350	0.07-0.15

3.5 Model verification and validation

Since there are two objects in the hydrodynamic interaction in this study, the panel strip of the ROV system and the panel mesh of the vessel are required. The mesh convergence analysis of vessel performed in this study is shown in Figure 3. The strip convergence analysis of ROV system performed in this study is shown in Figure 4. Because the coupled vessel and ROV model needs to be hydrodynamically analysed by time domain analysis, a convergence analysis for the time step is also necessary. The time step convergence analysis of coupled system performed in this study is shown in Figure 5.

Figure 3 is the first-order force of the offshore support vessel in different directions under different mesh number obtained. As the mesh number increases, the first-order forces in the heave, sway and roll directions continue to converge very fast. When the mesh number is larger than 20000, the first-order force in all directions converges.

Figures 4 is historical records of the tension in the cable connecting the ROV and TMS system with the service vessel under different strip number. Figures 5 is historical records of the tension under different time step. T1, T2 and T3 are different times for launching and recovering ROV and TMS system. T1 represents that the system is still in the air, T2 represents the descending stage, and T3 indicates that the system is fully submerged and still in water. When the number of strips is greater than 5, the tension in cable converges. In time domain analysis, the tension in cable converges when the time step is less than 0.006 s.

Ren et al. presented the tension in the connection line between wind turbine and support vessel in a single point mooring manner, and service vessel used in the literature and this study are the same [21]. The numerical model is further validated by comparison with first order force from the literature. The comparison between two results is shown in Figure 6 in which the first order force results are similar in different directions, and the maximum discrepancies between the two results does not exceed 1%.

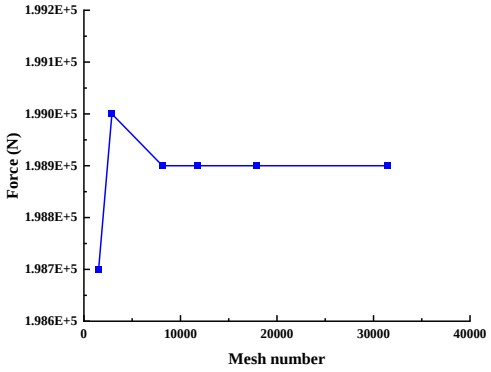

(a) Heave force of offshore support vessel

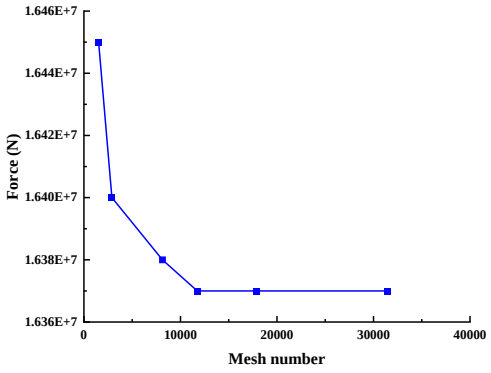

(b) Sway force of offshore support vessel

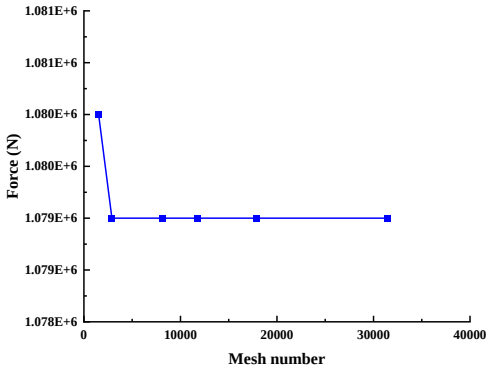

(c) Roll force of offshore support vessel

FIGURE 3: Mesh convergence of offshore support vessel panel model

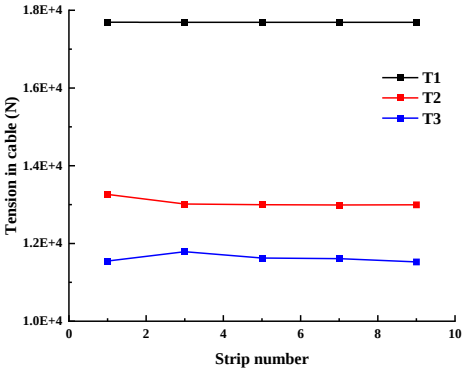

FIGURE 4: Strip convergence of the ROV and TMS system model

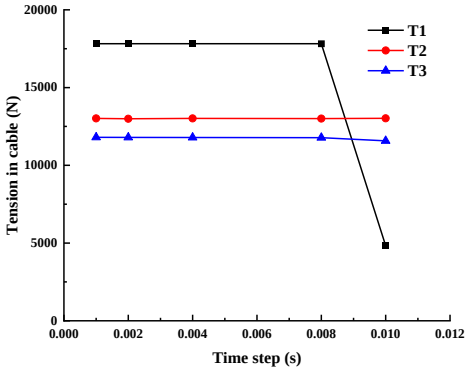

FIGURE 5: Time step convergence of time domain analysis

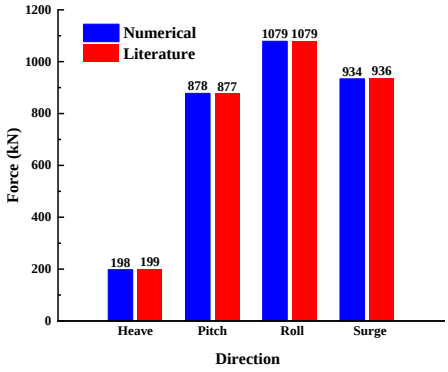

FIGURE 6: The comparison of first order force

4. RESULTS AND DISCUSSION

4.1 Stationary analyses in irregular sea

The maximum cable tension generally occurs when the lower part of the ROV is at still water level. At this time, the cable bears the weight of the ROV, and the lower part of the ROV is constantly impacted by waves, and the umbilical cable may bear a greater average tension and a sudden load occurs. Therefore, the steady-state analysis is carried out on the sea state

with the wave height of 1.0 m and the peak period of 3.5-5.0 s in the operational limit. For marine crane operations assumed to be performed within 30 minutes including contingency time. The ROV system maintains the position where the bottom touches the water surface, there is no winch speed, and the simulation time is 30 minutes. Table 7 shows brief statistics for the static analysis, while the time histories for each sea state are shown in Figure 7.

TABLE 7: Stationary analysis in different sea states

	Unit	Value			
Peak period	s	3.5	4.0	4.5	5.0
Mean of tension	N	16452.9	16403.0	16256.5	16160.4
Minimum cable tension	N	11407	11763	10859	10911
Maximum cable tension	N	22085	21693	21274	21537

According to time histories from stationary analysis in different sea states, the tension in the ropes often exceeds the weight of the system, which causes snap loads in the cables. The results in Table 7 show that as the wave period increases, the average, minimum and maximum of the cable tension have similar resultant values. The overall trend of the average and maximum values is slightly lower, which is due to the reduced probability of the ROV system being subjected to the maximum wave height. However, the tension in the rope was slightly higher at the 4.0 s period compared to the other wave periods, which may be due to the nonlinear behaviour of the transient loads and the large relative motion of the ROV and TMS systems to the crane in the 4.0 s sea state.

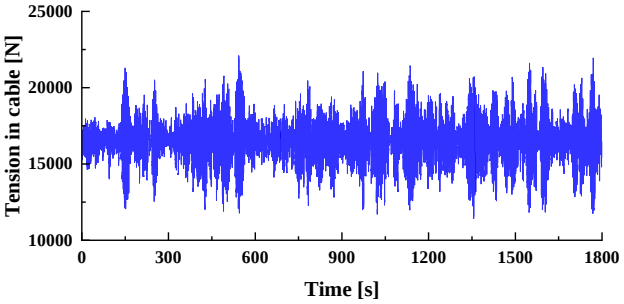

(a) Stationary analysis in irregular wave T_p= 3.5s

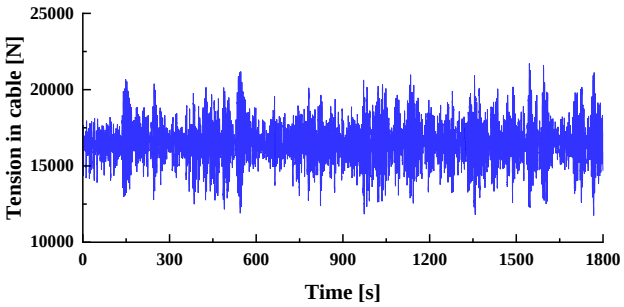

(b) Stationary analysis in irregular wave T_p= 4.0s

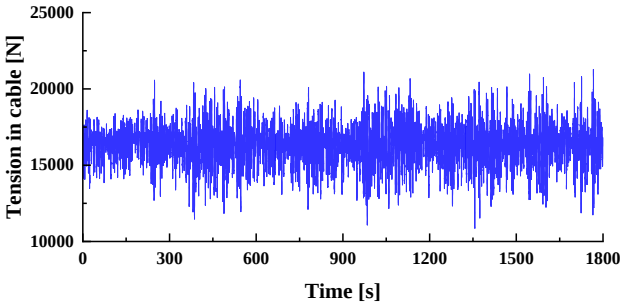

(c) Stationary analysis in irregular wave T_p= 4.5s

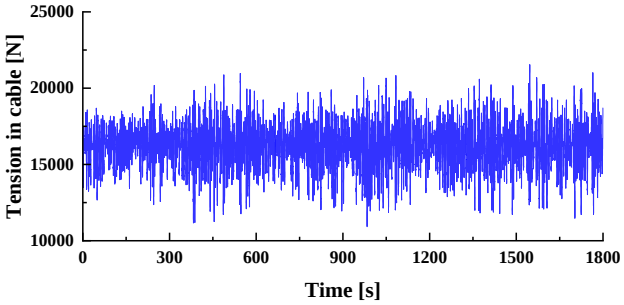

(d) Stationary analysis in irregular wave T_p= 5.0s

FIGURE 7: Time histories from stationary analysis in different sea states

4.2 Repeated lowering through wave zone

The launch and recovery of ROV mainly include two processes of descent and ascent. Because the sea conditions are irregular waves, the tension of the cable is not the same every time when descending and ascending. Multiple simulations are required for each sea state at each stage so that good estimates of maximum and minimum cable tensions can be obtained. Therefore, the analysis is performed for the same operationally limited sea conditions. The initial position of the ROV system is 7 m above the free surface. Before the crane is operated, the ROV system will be stationary for a period 10s in the initial position, and then the winch is started at a running speed of 0.5 m/s. When the ROV descends to a certain position where it is completely submerged, the winch stops, and 10 simulations are run for each sea state. The statistics for all sea state analysis are listed in Table

8, and the time histories of the cable tension for each sea state are shown in Figure 8.

TABLE 8: Time domain analysis of lowering in different sea states

	Unit	Value			
Peak period	s	3.5	4.0	4.5	5.0
Mean of tension	N	13449	13386.1	13392.3	13391.8
Minimum cable tension	N	3823.3	4127	3866.7	4231.4
Maximum cable tension	N	18555	18695	18990	19527

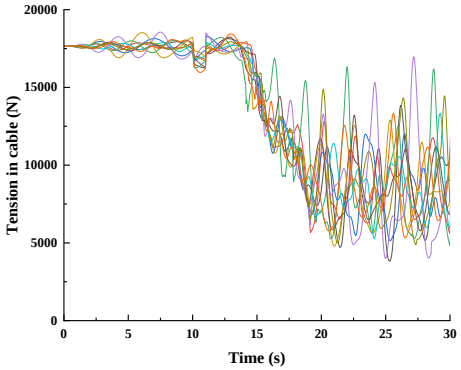

(a) Time histories of lowering in irregular wave T_p= 3.5s

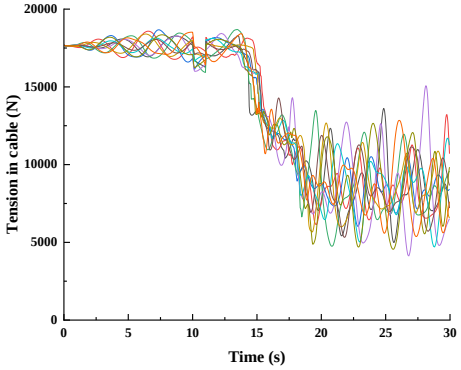

(b) Time histories of lowering in irregular wave T_p= 4.0s

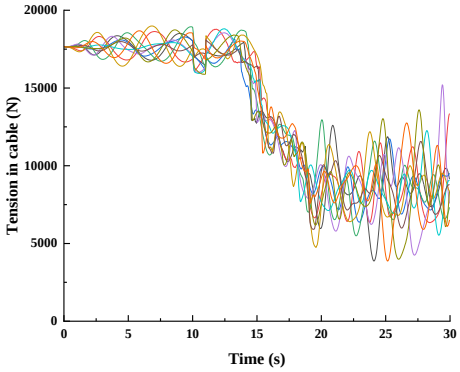

(c) Time histories of lowering in irregular wave T_p= 4.5s

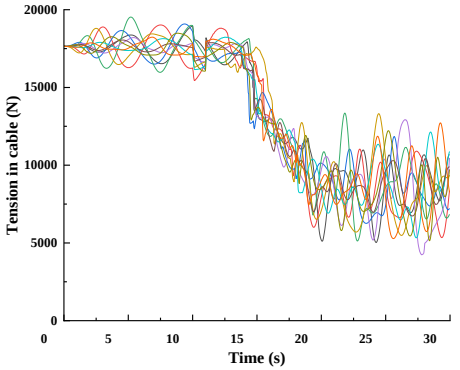

(d) Time histories of lowering in irregular wave T_p= 5.0s

FIGURE 8: Time histories of lowering in different sea states

The results in Table 8 show that as the peak period of the ocean wave increases, the average tension and the minimum tension of the rope remain basically stable, but the maximum tension continues to increase. As shown in Figure 8, at time 10 s, due to the sudden movement of the crane, there was a brief drop in the tension of the rope and then recovered. At 16 s and 17 s, the bottom of the ROV system had just touched the water surface, and there was a brief increase in cable tension due to the sudden loading caused by the slack umbilical. In the following 18-20 s, the tension of the rope will increase due to the impact force and quadratic drag. From the time history and statistical data, the sea state will have a loose umbilical phenomenon in the peak range of 15-19 s.

4.3 Repeated recovery through wave zone

During the ascent of the ROV system, the same software program, winch operating speed and the number of simulations were used. However, the ROV system was recovered from 25 m below the tip of the crane. The ROV system will be still for 10s in the initial position, and then the crane will start. Table 9 shows the results of the ascent procedure, while Figure 9 shows the time histories of recovering in different sea states.

TABLE 9: Time domain analysis of recovering in different sea states

	Unit	Value			
Peak period	s	3.5	4.0	4.5	5.0
Mean of tension	N	11278.5	11269.3	11299.5	11293.4
Minimum cable tension	N	7267.3	6361.6	6459.7	6225.2
Maximum cable tension	N	18733	19212	18946	18833

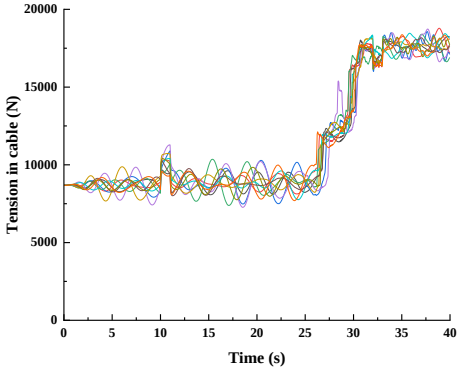

(a) Time histories of recovering in irregular wave T_p= 3.5s

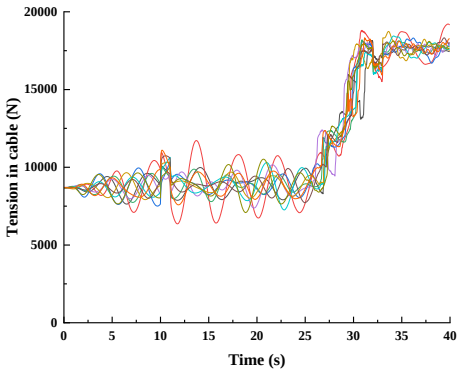

(b) Time histories of recovering in irregular wave T_p= 4.0s

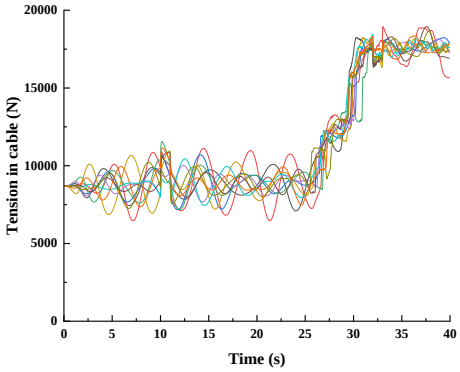

(c) Time histories of recovering in irregular wave T_p= 4.5s

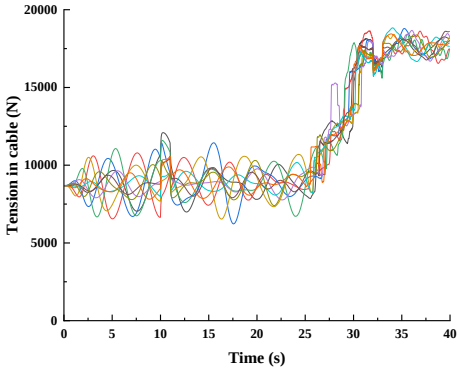

(d) Time histories of recovering in irregular wave T_p= 5.0s

FIGURE 9: Time histories of recovering in different sea states

It can be seen from Table 9 that when the ROV system rises, the change of peak period has little effect on the mean of tension and maximum cable tension of the rope. As shown in Figure 9, there is a sudden increase in the rope tension at 10 s, which is due to the sudden start of the winch. At about 32 s, the crane stopped running suddenly, and there was a sudden decrease in the rope tension due to the vertical upward inertia of the ROV system. When passing through the wave zone, due to exit forces and quadratic drag, slack of the umbilical occurs at about 26 s, resulting in a significant transient load. However, the umbilical tension may be subjected to greater snap loads during recovery compared to the launch phase of the ROV system.

4.4 Investigation of winch speed

Winch speed is an important parameter during launch and recovery of ROV systems. In addition to affecting control program time, slam force and drag are also affected. Because of the larger snap loads that occur during recovery, the influence of winch speed is investigated during recovery. Three common different winch speeds are operated under the significant wave height of 1 m and the peak period of 4.5 s, and other conditions are consistent with those in the repeated recovery through wave

zone. The statistic results are shown in Table 10, while Figure 10 shows the time histories of the cable tension in different winch speed. Because the conditions are the same, the results of time histories of lowering in winch speed 0.5 m/s is shown in section 4.3.

TABLE 10: Time domain analysis of lowering in different winch speed

	Unit	Value		
Winch speed	s	0.5	0.7	0.9
Mean of tension	N	11299.5	12398.3	13136.4
Minimum cable tension	N	6459.7	6854.1	6854.1
Maximum cable tension	N	18946	19091	18957

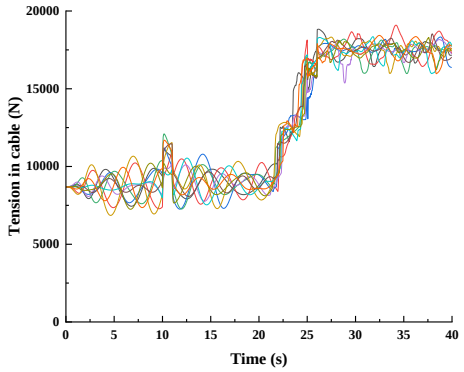

(a) Time histories of lowering in winch speed 0.7 m/s

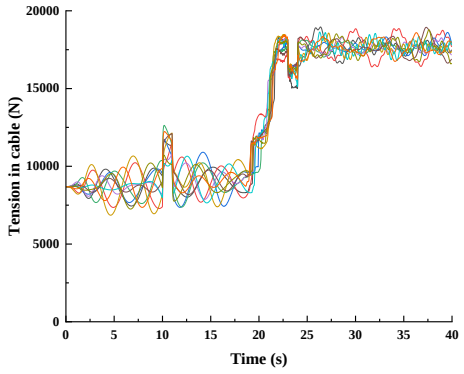

(b) Time histories of lowering in winch speed 0.9 m/s

FIGURE 10: Time histories of lowering in different winch speed

As the winch speed increases, the mean of tension and minimum cable tension of the cable will decrease due to resistance, as shown in Table 10. It can be obtained from Figure 10 that the change of rope tension at about 10 s and 24 s will increase with the increase of winch speed, which is caused by inertia. However, when ROV and TMS systems travel through wave zones faster at higher winch speeds, the system is exposed to wave forces for less time, which reduces the chance of cable slack.

The developed numerical model was validated in a wave tank with 1:10 scale model scale experimental results. In a prototype sinusoidal wave T_p = 7.91, H_s = 0.60 and winch speed 0.50 m/s, the simulation results are similar to the smoothed experimental results, as shown in Figure 11.

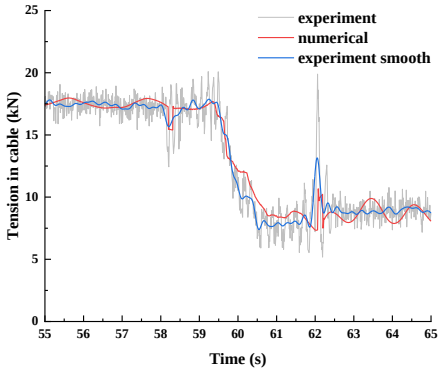

FIGURE 11: Comparison of numerical and experimental results

5. CONCLUSION

The coupling system of ROV and TMS system and offshore support vessel is studied based on numerical simulation. According to the environmental conditions measured during the O&M service of the offshore wind farm in the North Sea and the constraints of the ROV system operation, the tension of the connection lines under different conditions was explored. The current numerical model for time-domain coupling analysis was verified using experiments.

When the bottom part of the ROV and TMS system is in contact with still water, the connecting cables are likely to be under maximum tension as a result of snap loads caused by slack cables.

The maximum and average tensions of the cable under different conditions during the launch and recovery phases do not experience significant change, but the snap load due to umbilical slack tends to be greater during the ascending phase, indicating that the recovery phase is more critical for the operating conditions investigated.

In the case of a certain significant wave height, the winch speed has little effect on the maximum tension at different peak periods, but a higher winch speed can reduce the probability of snap load generation.

ACKNOWLEDGEMENTS

The authors would like to acknowledge all partners at the University of Strathclyde for their assistance in preparing this paper and their support for design and test experience on offshore structures.

REFERENCES

[1] Retrieved from: https://map.4coffshore.com/offshore wind/. [Accessed 5 December 2022].

[2] Chirosca, A.M., Rusu, L. and Bleoju, A., 2022. Study on wind farms in the North Sea area. Energy Reports, 8, pp.162-168.

[3] Lubis, M.B. and Kimiaei, M., 2021. Wave flume and numerical test on launch and recovery of ultra-deep-water ROV through splash zone under wave and ship motion. Ocean Engineering, 238, p.109767.

[4] Niedzwecki, J.M. and Thampi, S.K., 1988. Heave compensated response of long multi-segment drill strings. Applied Ocean Research, 10(4), pp.181-190.

[5] Driscoll, F.R., Lueck, R.G. and Nahon, M., 2000. The motion of a deep-sea remotely operated vehicle system: Part 1: Motion observations. Ocean Engineering, 27(1), pp.29-56.

[6] DNV, 2019. Modelling and analysis of marine operations. In: (Vol. DNVGL-RP-N103). Norway: Det Norske Veritas.

[7] Kimiaei, M., Khosroshahli, A.R., 2008. Dynamic amplification factors in lifting operations for installation of a subsea spool. In: Marine Operations Specialty Symposium (MOSS).

[8] Kimiaei, M., Xu, J., Yu, H., 2009. Comparing the results of a simplified numerical model with DNV Guidelines for installation of subsea platforms. In: International Conference on Ocean, Offshore and Arctic Engineering, Hawaii, USA.

[9] Valen, M., 2010. Launch and recovery of ROV: Investigation of operational limit from DNV Recommended Practices and time domain simulations in SIMO (Master's thesis, Institutt for marin teknikk).

[10] Bjerkholt, R.F., 2014. Analysis of ROV Lift Operation (Master's thesis, Institutt for marin teknikk).

[11] Jia, D. and Agrawal, M., 2014, May. Fluid-structure interaction: lowering subsea structure/equipment in splash zone during installation. In Offshore Technology Conference. OnePetro.

[12] Thurston, K.W., Swanson, R.C. and Kopp, F., 2011, January. Statistical characterization of slacking and snap loading during offshore lifting and lowering in a wave environment. In International Conference on Offshore Mechanics and Arctic Engineering (Vol. 44335, pp. 269-277).

[13] Lubis, M.B. and Kimiaei, M., 2021. Wave flume and numerical test on launch and recovery of ultra-deep-water ROV through splash zone under wave and ship motion. Ocean Engineering, 238, p.109767.

[14] SIMO Project Team (2013). SIMO - Theory Manual Version 4.0 rev. 3. Report 516412.00.03.

[15] Sayer, P., 2008. Hydrodynamic loads during the deployment of ROVs. Ocean Engineering, 35(1), pp.41-46.

[16] Kopsov, I.E. and Sandvik, P.C., 1995, June. Analysis of subsea structure installation. In The Fifth International Offshore and Polar Engineering Conference. OnePetro.

[17] Sandvik, P.C., Lieng, J.T. and Lunde, S., 1993. Analysis of the dynamics during installation of subsea structures.

[18] Sayer, P., 1996. Hydrodynamic forces on ROVs near the air-sea interface. International journal of offshore and polar engineering, 6(03).

[19] Øritsland, O., 1989. A summary of subsea module hydrodynamic data. Marine Operations.

[20] Oritsland, O. and Lehn, E., 1989. Hydrodynamic forces and resulting motion of subsea modules during lifting in the splash zone.

[21] Ren, X., Tao, L., Nuernberg, M. and Ramzanpoor, I., 2022, June. Interaction of offshore support vessel with adjacent offshore wind turbine during maintenance operation. In International Conference on Offshore Mechanics and Arctic Engineering (Vol. 85932, p. V008T09A027). American Society of Mechanical Engineers.